Engineering Fracture Mechanics 99 (2013) 87–100

Contents lists available at SciVerse ScienceDirect

Engineering Fracture Mechanics

journal homepage: www.elsevier.com/locate/engfracmech

Effects of laser energy on fatigue crack growth properties of 6061-T6 aluminum alloy subjected to multiple laser peening

S. Huang [a,b,*], J.Z. Zhou [a], J. Sheng [a], J.Z. Lu [a], G.F. Sun [a], X.K. Meng [a], L.D. Zuo [a], H.Y. Ruan [a,b], H.S. Chen [a]

[a] School of Mechanical Engineering, Jiangsu University, Zhenjiang 212013, PR China
[b] V-zenith Laser Technology Company, Zhenjiang 212013, PR China

ARTICLE INFO

Article history:
Received 18 May 2012
Received in revised form 16 January 2013
Accepted 25 January 2013

Keywords:
Laser peening
Residual stress
Effective stress intensity factor
Fatigue crack growth

ABSTRACT

Effects of laser energy on fatigue crack growth (FCG) properties of 6061-T6 aluminum alloy subjected to multiple laser peening (LP) were investigated. LP experiments and typical FCG experiments were performed on the compact tension (CT) samples. In order to reveal the enhancement mechanism of laser energy on FCG properties through residual stress (RS), a numerical model of effective stress intensity factor (SIF) was established. The results showed that compressive RS induced by LP can effectively decrease FCG rate and increase FCG lives of CT samples. The experimental results and numerical analysis correlated with each other.

1. Introduction

Fatigue crack growth (FCG) behaviors of engineering aluminum (Al) alloys are of great technological importance for ensuring fail-safe material design for structural applications [1,2]. Micro-cracks normally initiate in the surface of metallic material, and can be mitigated by inducing compressive residual stresses (RS) [3,4]. Existing literature shows that laser peening (LP) can significantly improve the fatigue performance by inducing high amplitude compressive RS on a number of metals and alloys [5–7]. The compressive RS induced by LP may cause the crack closure to incur the reduction of effective driving force for the FCG, which is favorable for the extension of FCG life [8,9]. Nowadays, many attentions have been paid to assess the effects of LP on FCG properties [10–14].

Zou et al. have discussed the effects of LP on the FCG rate of 2024-T62 Al [10], but they did not study the effects of laser energy on the FCG properties, and its strengthening effects were not ideal due to the small LP processing area and large spot distance along the crack tip. Rubio-Gonzalez et al. have examined the effects of laser pulse densities on FCG properties of 6061-T6 Al and 2205 duplex stainless steel, and they improved the LP path along the crack tip. The results showed that the FCG rate decreased and fracture toughness increased with the increased pulse density [11,12]. Liu et al. have studied the effects of laser power density on the fatigue life of 7050 Al alloy subjected to LP. Both the experimental and numerical results showed that a carefully chosen laser power density, when treating materials like aluminum alloys, can prevent internal cracking [13].

Laser energy or laser power density can greatly affect the FCG properties of the components [10–13], and the influence extent depends strongly upon the RS magnitude and distribution arising from LP [14–16]. Chahardehi et al. put forward the "Equivalent Fatigue Stress" to characterize stress intensity factor (SIF) under compressive RS field induced by LP [15]. The

* Corresponding author. Address: Xuefu Road 301, Jingkou District, Zhenjiang 212013, PR China. Tel.: +86 511 88786318; fax: +86 511 88780241.
E-mail address: huangshu11@sina.com (S. Huang).

0013-7944/$ - see front matter © 2013 Elsevier Ltd. All rights reserved.
http://dx.doi.org/10.1016/j.engfracmech.2013.01.011

Nomenclature

R	stress ratio
FCG	fatigue crack growth
SIF	stress intensity factor
RS	residual stress
da/dN	FCG rate
ΔK	SIF range
C	Paris law coefficient
m	Paris law exponent
a	crack length
N	total number of load cycles
a_0	initial crack length
a_c	critical crack length
a_f	final crack length
W	plate width
B	plate thickness
F	fatigue loads
$\sigma_{\max}$	maximum tensile stress
$\sigma(x)$	tensile stress
K_1	SIF caused by tensile loads
α	correction coefficient of K_1
K_2	SIF generated by RS induced by LP
I	incident laser power density
I_P	laser power density
$A(t)$	absorption coefficient
t	time
P	shock pressure
L	thickness L during laser irradiation
Z_i	shock impedance
ρ_i	density
D_i	shock velocity
i	opaque coating ($i = 1$) or transparent overlay ($i = 2$)
χ	correction factor of the ratio of thermal to plasma internal energy
γ	specific-heat ratio
T	laser switched-off time
τ	FWHM of laser pulses
HEL	Hugoniot elastic limit
σ^{dyn}	dynamic yield strength of the material
v	Poisson's ratio
ε_p	surface plastic strain
L_p	influence depth of RS
σ_{surf}	surface RS
λ,μ	Lame's constants
C_{e1}	elastic wave velocity
C_{p1}	plastic wave velocity
σ_0	initial surface RS
r_p	laser spot radius
σ_t	actual RS
σ_{ci}	calculated RS
β	correction coefficient of K_2
ΔK_1	SIF range of K_1
N_1	FCG lives of untreated CT samples
ΔK_2	SIF range of K_2
N_2	FCG lives of laser peened CT samples
$\Delta K_{2\text{-eff}}$	effective SIF range of K_2

study of Zhang et al. showed the effects of LP on SIF at the edge of the circular hole, and the results indicated that compressive RS near the hole had an important influence on the radial FCG when the applied stress was relatively low [16]. However, there remain technical challenges of accurately quantifying RS relaxation and redistribution under cyclic mechanical load, therefore, the effect mechanism of LP on the fatigue behavior has not yet been fully identified. It is necessary to undertake

further experimental and numerical investigation to reveal the enhancement mechanism of RS induced by different LP energy on FCG properties.

In this study, multiple LP experiments and typical fatigue tests are performed on 6061-T6 Al compact tension (CT) samples with different laser energy, and then the RS distribution, microstructure on the fracture surface, FCG rate and FCG lives are discussed. In order to reveal the effect mechanism of laser energy on FCG properties through the RS, the numerical model of the effective SIF induced by LP is established, and the predicted model of FCG life is derived. In addition, a comparison is carried out between the experimental results and numerical analysis, which will provide useful information for the industrial application of LP.

2. Experiment methods

2.1. Experimental material and sample

6061-T6 Al alloy was selected in this work. Its chemical composition is: 0.90 wt.% Mg, 0.62 wt.% Si, 0.33 wt.% Fe, 0.28 wt.% Cu, 0.17 wt.% Cr, 0.06 wt.% Mn, 0.02 wt.% Ti, 0.02 wt.% Zn, and the mechanical properties are shown in Table 1. The CT samples used for FCG tests are as illustrated in Fig. 1. All the CT samples are processed with the loading axis parallel to the rolling direction. Before the process of LP, a fatigue pre-crack of 2.5 mm long (from notch tip) was formed on each sample by a MTS-809 servo-hydraulic system at room temperature (25 °C) in the air. The load ratio was maintained at $R = 0.5$ and the frequency was 9 Hz with tensile sinusoidal form. Therefore, the total length of the initial crack was 15 mm after pre-cracking.

2.2. LP processing

A high energy shockwave was induced by a Q-switched Nd: YAG laser system at the Laser Technology Institute of Jiangsu University, operating at 5 Hz repetition-rate with a wavelength of 1064 nm. The pulse duration was 10 ns in FWHM and a quantitative spatial laser beam profile was shown in Fig. 2. The laser beam was focused by a convergent lens (focal length = 1800 mm), the horizontal position of which can be adjusted to obtain the desired spot diameter (3 mm) and laser energy working together with a variable laser controller. Table 2 shows the processing parameters used in two-sided LP. During the process of LP, laser energies of 3 J, 5 J and 7 J were selected, and the overlapping rate between the adjacent spots was 50% with the total LP region of 15 mm × 15 mm. A water curtain with a thickness of 1–2 mm was used as the transparent confining layer and the professional Al foil with a thickness of 100 μm was used as an absorbing layer to protect the surface of samples from thermal effects. Fig. 1 shows the LP treatment regions, as well as the swept direction of CT samples. Fig. 3 shows the typical 6061-T6 CT samples subjected to LP with different laser energy.

2.3. FCG testing

The FCG tests were performed on a MTS-809 servo-hydraulic system at the room temperature (25 °C) in the air. The maximum external load was maintained at 3.0 kN and load ratio R was 0.5. The frequency of 5 Hz with a tensile sinusoidal form was used. The whole FCG testing process was monitored using a COD silicon chuck in order to obtain the FCG properties under different cycles. Twelve samples were selected. Samples 1–3 were not treated with laser peening, samples 4–6, 7–9 and 10–12 were peened with the laser energies of 3 J, 5 J and 7 J, respectively. The average value of three samples in each group was taken to analyze. Typical photos of the FCG testing were shown in Fig. 4.

2.4. Measurements of RS and microstructures

The RS were determined by the X-ray diffraction with the $\sin^2\psi$ method. Prior to the measurement of RS along the depth direction, the electro-polishing material removal method was used. An X-ray tube with a chrome anode operated at 20 kV and 5 mA was used. The X-ray beam diameter was about 1 mm. The X-ray source was Cr Kα ray and the diffraction plane was α phase (3 1 1) plane in the stress calculation. The scanning angle of $2\theta_\psi$ was from 135.5° to 142.5° with step angle of 0.1° s^{-1} and present time (time per measurements) of 1.5 s. The fatigue fracture microstructure of the untreated and laser peened samples were analyzed by a JSM-6700F JEOL scanning electron microscopy (SEM).

Table 1
Mechanical properties of 6061-T6 aluminum alloy.

Yield strength $\sigma_{0.2}$ (MPa)	Tensile strength σ_b (MPa)	Elongation δ%	Elastic modulus E (GPa)	Specific gravity ρ (kg/m^3)	Possion's cofficient, v
289.9	328	13.5	69.8	2672	0.33

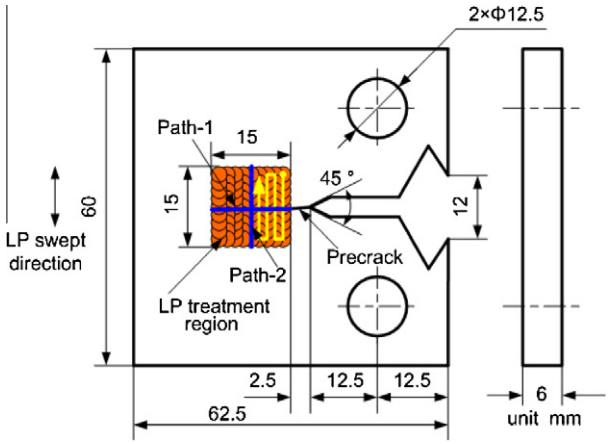

Fig. 1. The LP treatment region and swept direction of CT sample used in the FCG test.

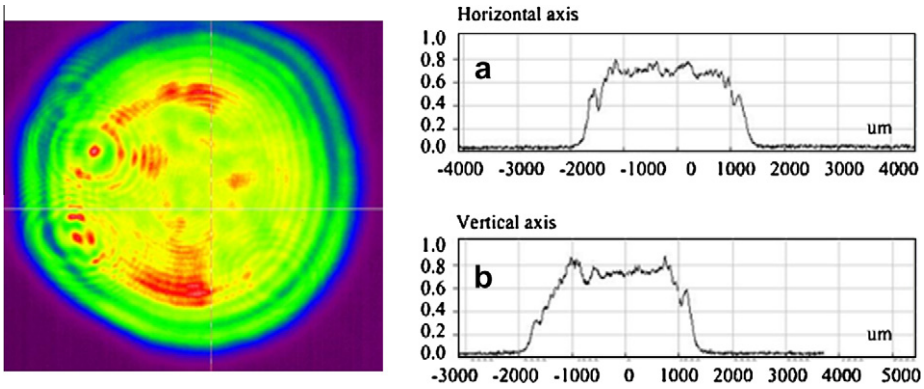

Fig. 2. A quantitative spatial laser beam profile: (a) horizontal axis and (b)vertical axis.

Table 2
The processing parameters used in multiple LP.

Parameters	Value
Beam divergence of output (mrad)	⩽0.5
Spot diameter (mm)	3
Pulse width (ns)	10
Repetition-rate (Hz)	5
Laser wavelength (nm)	1064
Laser energy (J)	3, 5, 7
Export stability	⩽±5%

3. Experimental results and discussion

3.1. RS distribution

Usually, the RS components of S_1 (parallel to pulse swept direction) and S_2 (perpendicular to pulse swept direction) should be considered. While since the applied load direction is parallel to pulse swept direction, S_1 will mainly offset the applied load, as a result, S_1 are reported along paths 1 and 2. Fig. 5a shows the surface RS distribution along Path 1 (as shown in Fig. 1) after LP. It is observed that the tensile RS with a value of 98 MPa appears at the crack tip of the untreated sample after pre-cracking, and it gradually becomes stable in the region of 7 mm away from the crack tip, with the value of 42 MPa. While the RS present compressive state along Path 1 after LP. The RS are −92 MPa, −117 MPa, and −158 MPa at the crack tip, and then they gradually increases to −168 MPa, −206 MPa and −225 MPa after 3 J, 5 J and 7 J LP, respectively. Fig. 5b shows the surface RS distribution along Path 2, it indicates that the RS distribution change from tensile state to compressive state

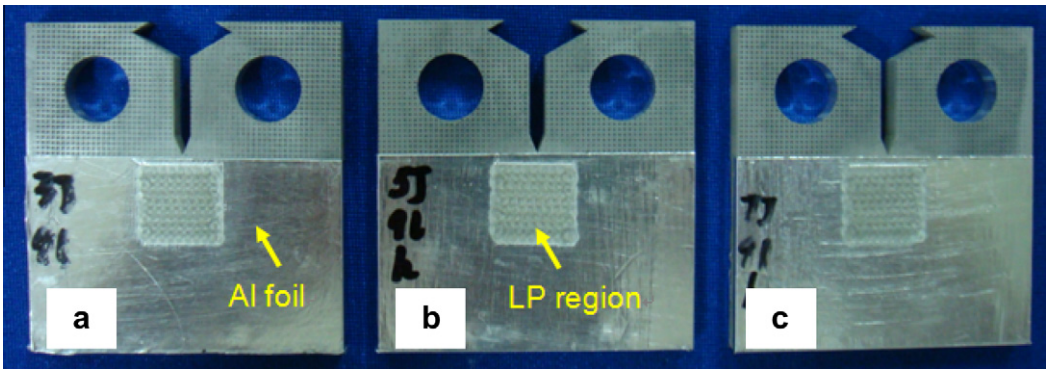

Fig. 3. Typical 6061-T6 CT samples subjected to LP with different laser energy. (a) 3 J, (b) 5 J and (c) 7 J.

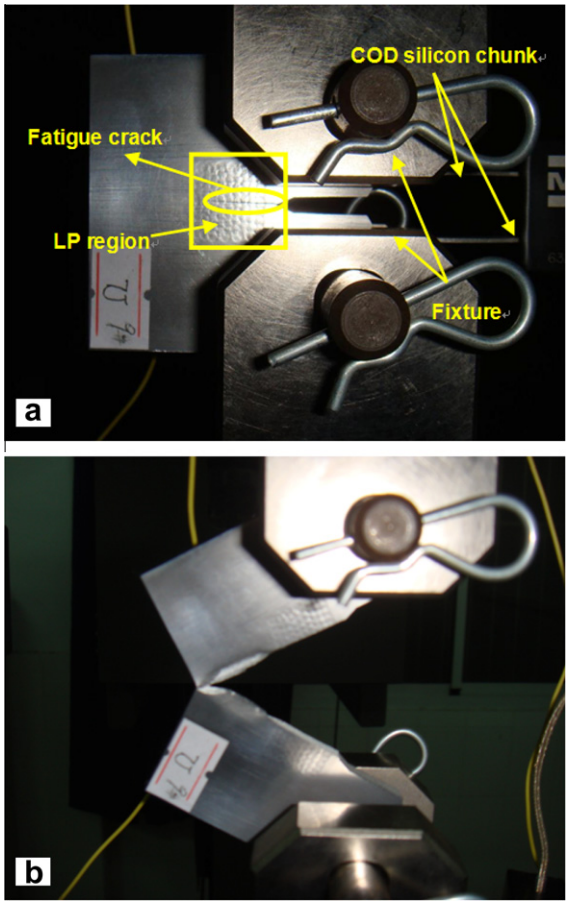

Fig. 4. Typical photos of FCG testing on 6061-T6 CT sample after LP: (a) during FCG and (b) instantaneous fracture.

after LP, and the values of compressive RS increase with the increase of laser energy. However, the maximum surface compressive RS increase by 21.71% and 8.92% when the laser energy increases from 3 J to 5 J and from 5 J to 7 J, respectively, indicating that the increment of surface RS gradually reach the saturated state as laser energy increases.

Fig. 6 shows the distributions of RS as a function of depth on 6061-T6 Al alloy subjected to different laser energy. It is observed that the significant compressive RS mainly exists in the near-surface regions in all cases, and the maximum value is located at the top surface. The maximum values of surface compressive RS after 3 J, 5 J and 7 J LP are −175 MPa, −213 MPa and −232 MPa, and the corresponding depths of compressive RS are 0.48 mm 0.55 mm and 0.61 mm, respectively. It can be seen that the higher laser energy has a beneficial effect on the RS levels in the superficial layers. High amplitude compressive

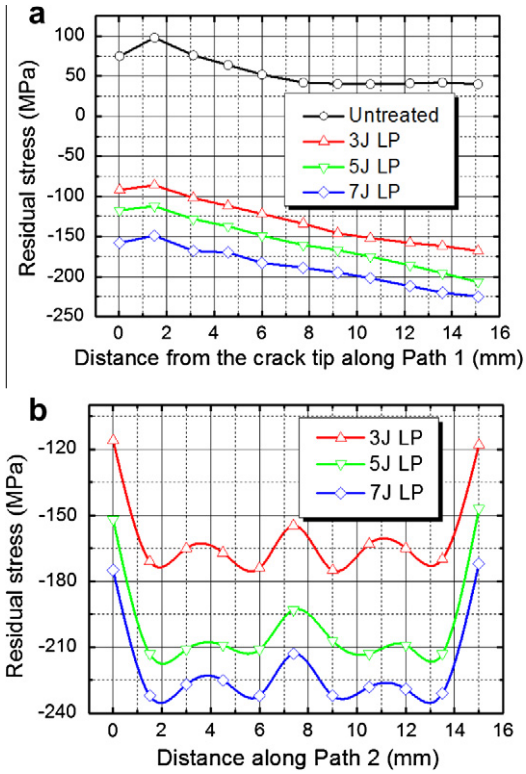

Fig. 5. RS distribution of (a) along the Path 1 and (b) along the Path 2 subjected to different laser energy.

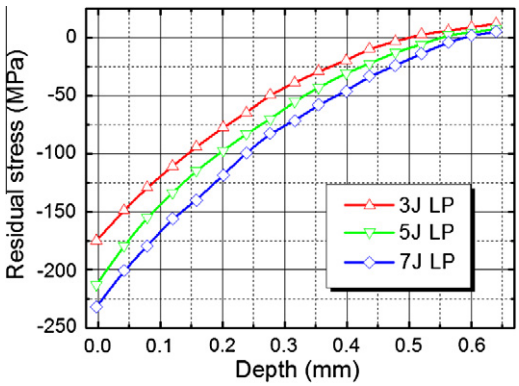

Fig. 6. RS distribution as a function of depth subjected to different laser energy.

RS can be induced by crystal defects such as high density and homogeneous dislocation, which is the main factor for greatly improving fatigue limits and dropping the fatigue gap sensitivity [6,7,17,18].

3.2. FCG path and microstructure on the fracture surface

The FCG behavior of the CT sample is typical of most conventional metallic samples, where cracking initiates at the machined notch tip and grows to failure under continual fatigue cycling. Generally speaking, the morphology of fatigue fracture is the direct result of material progressive wreck [19], and the spacing of fatigue striations can reflect the change of FCG rate *da*/*dN*. Fig. 7a–d shows the FCG path and microstructure on fracture surface at the depth of about 0.5 mm through the thickness of untreated and laser peened samples, when the crack reaches 25 mm in length. The fatigue striations can be clearly observed on the fracture surface of all the samples. Fig. 7a shows the spacing of the fatigue striation in the untreated CT sample is 0.77 μm, however, it decreases to 0.38 μm, 0.31 μm and 0.18 μm after 3 J, 5 J and 7 J LP, respectively (as shown in

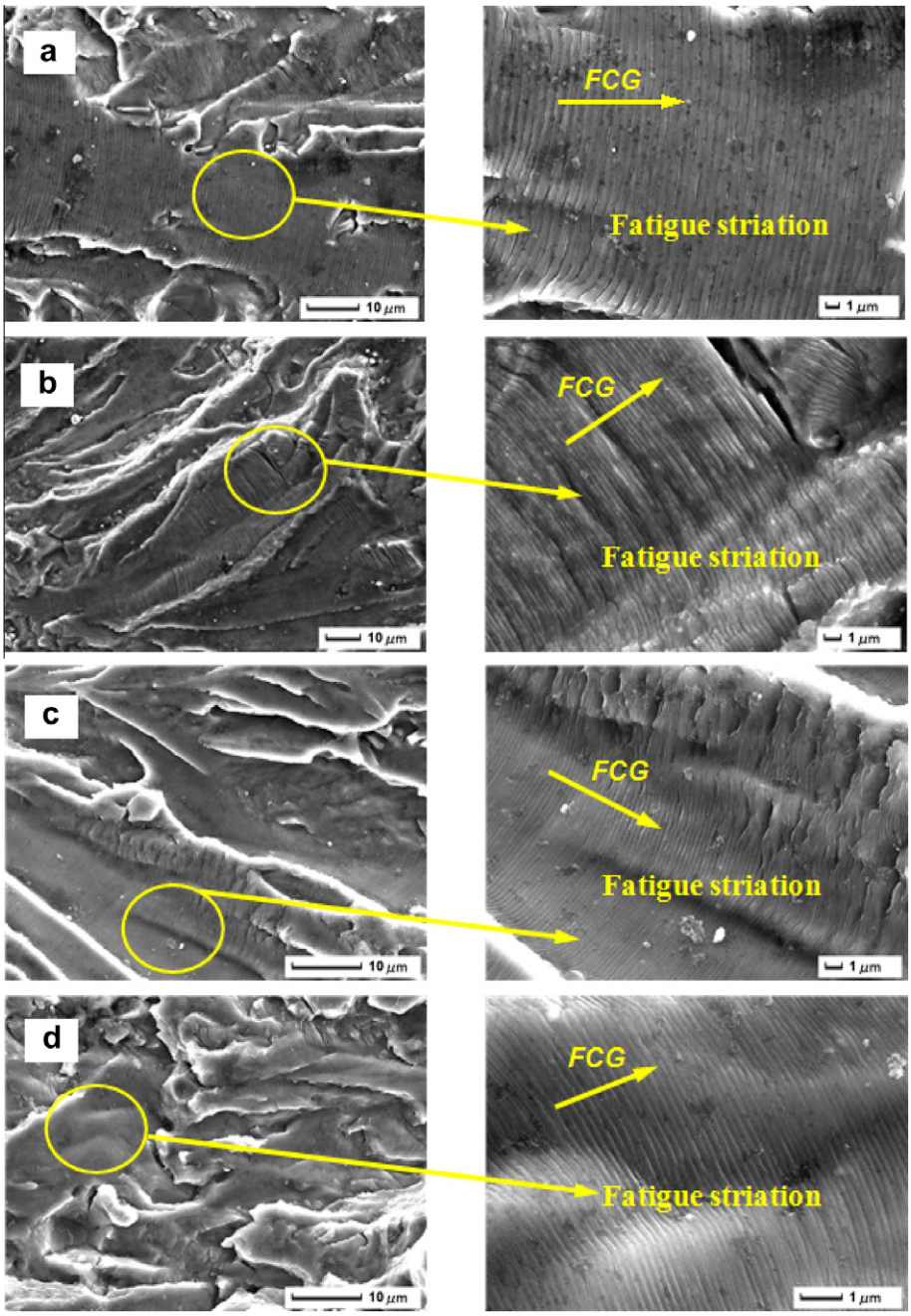

Fig. 7. Fatigue striation and FCG path on the fracture surface of (a) untreated, (b) 3 J laser-peened, (c) 5 J laser peened and (d) 7 J laser peened 6061-T6 CT samples.

Fig. 7b–d). The decrease of the fatigue striation spacing indicates the decrement of FCG rate. Compressive RS in the superficial layers induced by LP can reduce the actual SIF as well as the FCG rate of the crack tip [20,21], so LP can effectively improve the FCG resistance and relieve the negative effects of the crack initiation and propagation on 6061-T6 CT samples.

3.3. FCG lives

Fig. 8 shows the curves of crack length a versus cycles N on 6061-T6 CT samples subjected to different laser energy. It can be seen that the initial crack length of all the samples is 15 mm after pre-cracking. During the FCG testing process, crack length was monitored by a COD silicon chuck, and the final lives were calculated for the final instantaneous fracture length

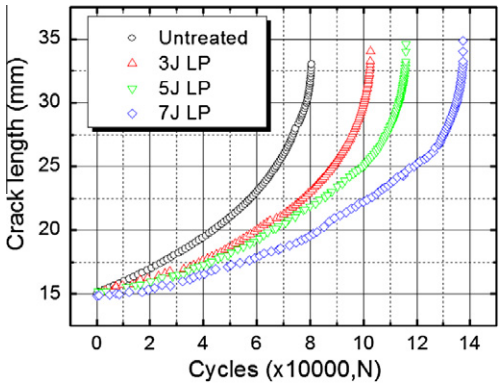

Fig. 8. Experimental curve of crack length a versus cycles N subjected to different laser energy.

of CT sample obtained by COD silicon chuck, as shown in Fig. 4b. When the crack length increases to 33.47 mm, the untreated sample is pulled off with the final fatigue lives of 80477 cycles, while the treated samples continue to expand to 34.46 mm, 34.63 mm and 34.87 mm after 3 J, 5 J and 7 J LP, with the corresponding fatigue lives of 102,687, 115,963 and 137,422 cycles, respectively. From the above-mentioned results, it can be seen that LP with laser energy changes from 3 J to 7 J can obviously increase the fatigue lives of 6061-T6 Al alloy by 27.60–70.76% compared with the untreated samples.

3.4. FCG rate

The complete curve of FCG rate can be qualitatively divided into three sections: The near threshold, stable expanding and rapidly expanding region. We mainly studied the FCG performance of 6061-T6 CT samples during the crack stable expanding region in this study. Fig. 9 shows the experimental curve of FCG rate da/dN as a function of SIF range ΔK, which can be regarded as linear under the logarithmic coordinates. The Paris formula is adopted to fit the relationship of the curves, and the changes of constant values of C and m can be found in Table 3. It indicates that C decreases while m increases with the increase of laser energy. Similar slope changes have been reported in previous crack propagation studies [22,23]. The laser peened samples result in a reduction of FCG rate when compared with the untreated samples, and it can be indicated by the decline of da/dN and ΔK curves. The reduction of da/dN is obvious in the initial period of FCG. However, when ΔK increases to high values in the final period of FCG, the FCG rate of all the samples are almost the same.

It indicates that the improvement of FCG resistance induced by LP can be separated into a relatively large increase in the initial FCG stage and a slight increase in the final FCG stage. In the initial FCG stage, compressive RS induced by LP can cause the crack closure and incur the reduction of effective driving force, which is favorable for the reduction of ΔK and da/dN [15,16,24]. Moreover, laser energy significantly affect the FCG rate in the initial FCG stage, the decrement of da/dN induced by 7 J LP is more evident than 5 J LP and 3 J LP. It is attributed to the introduction of higher compressive RS distribution perpendicular to the crack growth direction [25]. However, compressive RS release with the increasing of crack length, and the decrement of FCG rate weakens. Even in the laser peened samples, the crack arrest effects in the final FCG stage are limited, since the crack driving force is much larger than the resistance induced by compressive RS.

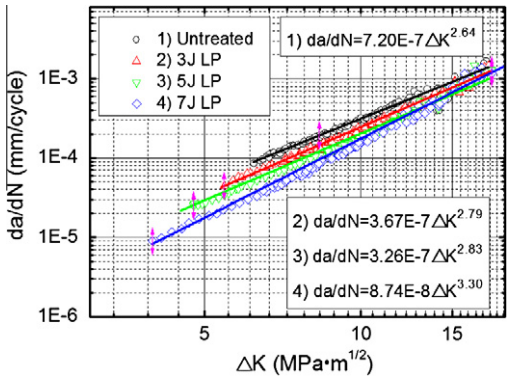

Fig. 9. Experimental curve of the SIF range ΔK versus FCG rate da/dN subjected to different laser energy.

Table 3
Material constants C and m of the untreated and laser peened samples.

Laser energy	Untreated	3 J LP	5 J LP	7 J LP
C (experimental)	7.20E−7	3.67E−7	3.26E−7	8.74E−8
m (experimental)	2.64	2.79	2.83	3.30
C (numerical)	6.81E−7	3.39E−7	2.81E−7	8.35E−8
m (numerical)	2.66	2.84	2.86	3.30

4. Numerical analysis of RS on FCG properties induced by LP

Geometry model and related instructions of CT samples are shown in Fig. 10, where a_0 and a_f refer to initial crack length and final crack length, and a represents instantaneous crack length at any time, W and B are width and thickness of sample, F is fatigue loads.

4.1. SIF K_1 caused by tensile loads

Fatigue tensile loads F exerted on both ends of CT samples, and the loading area in crack tip can be expressed as $B(W-a)$. Assuming that maximum tensile stress $\sigma_{\max}$ appears at the crack tip, and tensile stress $\sigma(x)$ will reduce to zero according to the linear relationship, as shown in Fig. 10, it can be concluded according to the static balance principle that,

$$FW = \int_0^{W-a} \sigma(x)B(W-a-x)dx = \int_0^{W-a} \frac{\sigma_{\max}B(W-a-x)^2}{(W-a)}dx \tag{1}$$

The solution of Eq. (1) is,

$$\sigma_{\max} = \frac{3FW}{B(W-a)^2} \tag{2}$$

In order to reduce the calculated error of the predictive model, correction coefficient α is introduced, and then the SIF of crack tip K_1 caused by tensile loads can be calculated by,

$$K_1 = Y\sigma\sqrt{\pi a} = \frac{3\alpha FW\sqrt{\pi a}}{B(W-a)^2} \tag{3}$$

4.2. SIF K_2 generated by RS induced by LP

One-dimensional model proposed by Fabbro et al. [26] was adopted to predict the shock pressure profile. A portion of the incident laser power density $I(t)$ is absorbed by the plasma as,

$$I_P(t) = A(t)I(t) \tag{4}$$

where $A(t)$ is the absorption coefficient and t is the time. The shock pressure P and thickness L during laser irradiation are calculated as functions of time t with following equations:

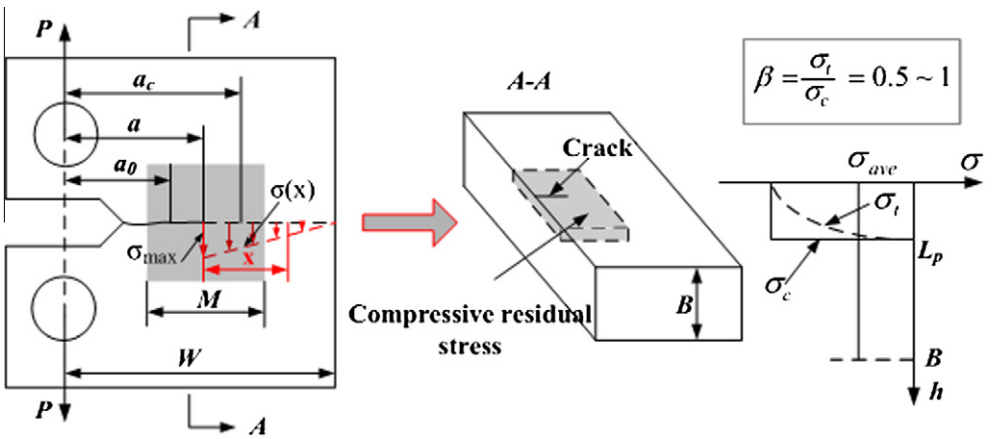

Fig. 10. Geometry model and related instructions of CT samples.

$$\frac{dL(t)}{dt} = \frac{2}{Z}P(t) \tag{5}$$

$$\frac{2}{Z} = \frac{1}{Z_1} + \frac{1}{Z_2} \tag{6}$$

$$I_P(t) = P(t)\frac{dL(t)}{dt} + \frac{3}{2\chi}\frac{d}{dt}[P(t)L(t)] \tag{7}$$

the shock impedance Z_i is defined as $Z_i = \rho_i D_i$, where ρ_i and D_i are the density and the shock velocity, respectively. The subscripts i represents opaque coating ($i = 1$) or transparent overlay ($i = 2$). The plasma is considered to be perfect gas with correction factor χ corresponding to the ratio of the thermal to plasma internal energy.

Assuming adiabatic cooling of the plasma, P and L after laser irradiation can be obtained by solving following equations coupled with Eqs. (4)–(7),

$$P(t) = P(T)\left(\frac{L(T)}{L(t)}\right)^{\gamma} \tag{8}$$

$$L(t) = L(T)\left(1 + \frac{\gamma+1}{2\tau}(t-T)\right)^{1/\gamma+1} \tag{9}$$

where γ is the specific-heat ratio, T is the laser switched-off time defined as $T = 2\tau$, and τ is the FWHM of laser pulses.

The shock pressure was solved numerically with the laser pulse profile and material properties according to the experimental conditions, as shown in Fig. 11.

Hugoniot elastic limit (*HEL*) can be calculated by [27]

$$HEL = \frac{1-v}{1-2v}\sigma^{dyn} \tag{10}$$

Where, v is Poisson's ratio, σ^{dyn} is the dynamic yield strength of the material under high strain rate.

During the process of LP, as the shock pressure increases to the dynamic yield strength, plastic deformation appears in a certain depth [28,29]. The surface plastic strain ε_p, influence depth of RS L_p and surface RS σ_{surf} can be calculated by [30],

$$\varepsilon_p = \frac{-2HEL}{3\lambda + 2\mu}\left(\frac{P}{HEL} - 1\right) \tag{11}$$

$$L_p = \left(\frac{C_{el}C_{pl}\tau}{C_{el} - C_{pl}}\right)\left(\frac{P - HEL}{2HEL}\right) \tag{12}$$

$$\sigma_{surf} = \sigma_0 - \left[\frac{\mu\varepsilon_p(1+\upsilon)}{(1-\upsilon)+\sigma_0}\right]\left[1 - \frac{4\sqrt{2}}{\pi}(1+\upsilon)\frac{L_p}{r_p\sqrt{2}}\right] \tag{13}$$

where λ and μ represent the Lame's constants. C_{e1} and C_{p1} refer to elastic and plastic wave velocities respectively, σ_0 is initial surface RS and r_p is the spot radius.

RS distribution with a size of $M \times M$ is assumed to generated on the surface of CT samples (gray rectangular area in Fig. 10), σ_t and σ_c are actual and calculated RS respectively, the RS along depth direction is equalized to calculate the SIF generated by LP,

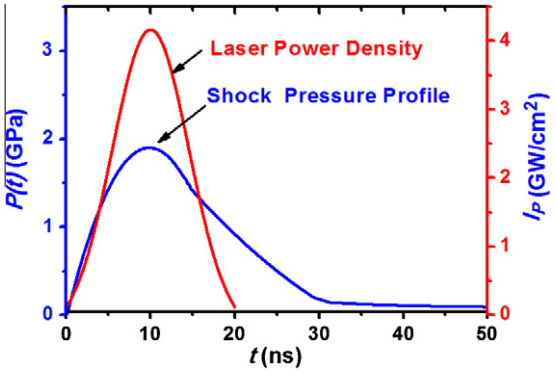

Fig. 11. Temporal profile of laser intensity and shock pressure ($A(t) = 0.9$, $\chi = 0.1$).

$$K_2 = \frac{\sigma_t L_p \sqrt{\pi a}}{B} = \frac{\beta \sigma_c L_p \sqrt{\pi a}}{B} \tag{14}$$

where β is introduced as an error correction coefficient, it is used to eliminate the calculated error when RS along the depth direction is simplified.

4.3. FCG lives of untreated CT samples

Assuming that crack growth of untreated and laser peened CT samples are always in stable expanding area which follows Paris formula [31],

$$\frac{da}{dN} = C(\Delta K)^m \tag{15}$$

According to Eq. (3), SIF range ΔK_1 of untreated CT samples is,

$$\Delta K_1 = \frac{3\alpha(1-R)F_{\max} W \sqrt{\pi a}}{B(W-a)^2} \tag{16}$$

Combining Eq. (15) with Eq. (16), FCG lives of untreated CT samples can be described as,

$$N_1 = \frac{B^m}{C[3\alpha(1-R)F_{\max} W \sqrt{\pi}]^m} \int_{a_0}^{a_f} \left[\frac{(W-a)^2}{\sqrt{a}}\right]^m da \tag{17}$$

4.4. FCG lives of laser peened CT samples

Since the additional SIF K_2 is introduced at the crack tip of laser peened CT samples, the maximum effective SIF $K_{2\text{max-eff}}$ after LP can be described as,

$$K_{2\,\text{max-eff}} = K_{1\,\max} - K_2 \tag{18}$$

It is supposed that crack grows only when SIF is positive, but closes when SIF is negative, so the minimum effective SIF $K_{2\text{min-eff}}$ can be expressed as,

$$K_{2\,\text{min-eff}} = \begin{cases} K_{1\,\min} - K_2 & (K_{1\,\min} \geqslant K_2) \\ 0 & (K_{1\,\min} < K_2) \end{cases} \tag{19}$$

Combining Eqs. (3), (14) with Eq. (19), effective SIF range $\Delta K_{2\text{-eff}}$ of laser peened CT samples is,

$$\Delta K_{2\text{-eff}} = \begin{cases} K_{1\,\max} - K_{1\,\min} = \frac{3\alpha(1-R)F_{\max} W \sqrt{\pi a}}{B(W-a)^2}, & K_{1\,\min} \geqslant K_2 \\ K_{1\,\max} - K_2 = \frac{3\alpha F_{\max} W \sqrt{\pi a}}{B(W-a)^2} - \frac{\beta \sigma_c L_p \sqrt{\pi a}}{B}, & K_{1\,\min} < K_2 \end{cases} \tag{20}$$

Eq. (20) demonstrates that $K_{1\text{min}}$ is less than K_2 during the initial period of FCG. As a result, compressive RS induced by LP can completely offset the tensile stress, which can retard the crack propagation. However, $K_{1\text{min}}$ is greater than K_2 in the final period of FCG, it is inapplicable for compressive RS to offset tensile stress, so there is no crack inhibition by LP. In addition, when $K_{1\text{min}}$ equals to K_2, a critical crack length a_c can be calculated, and the effects of LP on retarding FCG are weak if the crack length exceeds a_c. Combining Eq. (15) with Eq. (20), the FCG lives after LP can be calculated as,

$$N_2 = \int_{a_0}^{a_c} \frac{1}{C\left[\frac{3\alpha F_{\max} W \sqrt{\pi a}}{B(W-a)^2} - \frac{\beta \sigma_c L_p \sqrt{\pi a}}{B}\right]^m} da + \int_{a_c}^{a_f} \frac{1}{C\left[\frac{3\alpha(1-R)F_{\max} W \sqrt{\pi a}}{B(W-a)^2}\right]^m} da \tag{21}$$

5. Comparison of experimental and numerical results on FCG properties

Combining the numerical analysis with the experimental parameters such as material constants C and m (as shown in Table 3), the FCG lives and FCG rate of untreated and laser peened 6061-T6 CT samples can be estimated.

5.1. Comparison of FCG lives

According to Eqs. (17) and (21), the numerical curves of crack length a versus FCG lives N are obtained, as shown in Fig. 12. It is observed that the final FCG lives of the untreated CT samples are 80174 cycles, and then increased by 25.82%, 37.23% and 63.51% for the CT samples treated by 3 J, 5 J and 7 J LP, respectively. It indicates that compressive RS induced at the superficial layer by LP can obviously extend the FCG lives of CT samples, and life extension effects enhanced by the increase of laser energy.

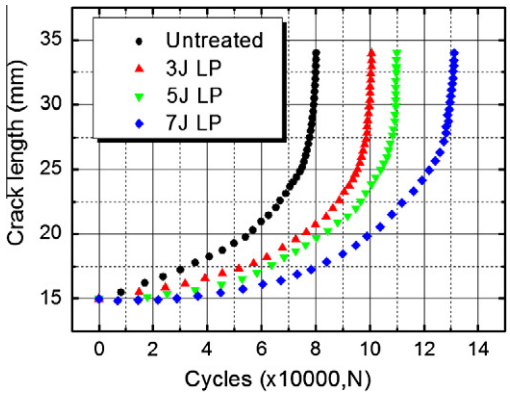

Fig. 12. Numerical curve of crack length a versus cycles N subjected to different laser energy.

Fig. 13 compares the numerical a–N curves with the experimental curves (as shown in Fig. 8) on CT samples subjected to different laser energy, it is found that the trends of numerical and experimental curves is similar. Especially, a good degree of consistency has been observed for the untreated samples in the reflection of the self-consistency of the numerical process. The errors of the final cycles to failure between the numerical and experimental results increase to 1.77%, 5.12% and 4.61% after 3 J, 5 J and 7 J LP, respectively, due to the simplification of numerical model and the heterogeneity of the material.

5.2. Comparison of FCG rate

The numerical curve of SIF range ΔK as a function of crack length a is shown in Fig. 14. ΔK of the untreated and laser peened CT samples can be obtained using Eqs. (16) and (20), respectively. The critical crack length can be calculated by setting $K_{1\min}$ equal to K_2. It is observed that in the initial period of FCG, the effective SIF range of laser peened samples is much lower than the untreated cases. The compressive RS will superimpose on the tensile applied stress, which results in a total stress lower than the externally applied stress [32,33]. During the process of FCG, it is found that the critical crack length in the laser peened samples increases with the increase of laser energy, which could be attributed to the higher value compressive RS. However, in final period of FCG, ΔK with and without LP does not change so much since the compressive RS releases as the crack grows [34,35].

Table 3 shows the comparison of the experimental and numerical change in the parameters of the Paris law, similar change tendency can be found, C decreases while m increases with the increase of laser energy. Fig. 15 shows the numerical curve of SIF range ΔK versus FCG rate da/dN, compared with the experimental curve of ΔK versus da/dN as shown in Fig. 9, it can be seen that although there exist some deviation from the experimental values, the numerical change tendency is coincident with the experiment results. In initial period of FCG, the FCG rate of laser peened samples is much slower than the untreated samples, and da/dN reduced with the increase of laser energy. However, in final period of FCG, the FCG rate of samples with and without LP is almost the same. This property and capability are critical because major RS relaxation takes place during the early stage as observed in previous studies [34–36].

It indicates that the proposed numerical model is able to predict the effect of RS induced by different laser energy on fatigue performance, which can deepen the understanding of strengthening mechanism induced by LP. However, calculated errors still exist due to the simplification of numerical model and the heterogeneity of the material. Therefore, further experimental and theoretical researches on cycle-dependent RS relaxation are required to improve the numerical model.

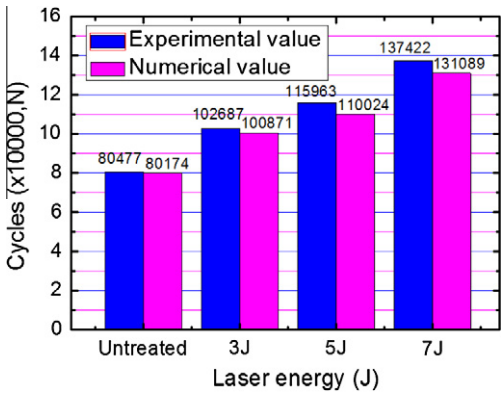

Fig. 13. Comparison of the experimental and numerical FCG cycles N subjected to different laser energy.

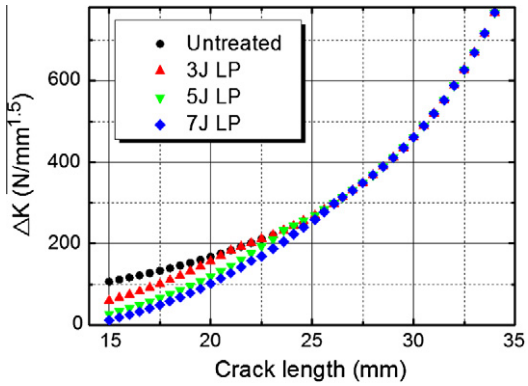

Fig. 14. Numerical curve of the crack length a versus SIF range ΔK subjected to different laser energy.

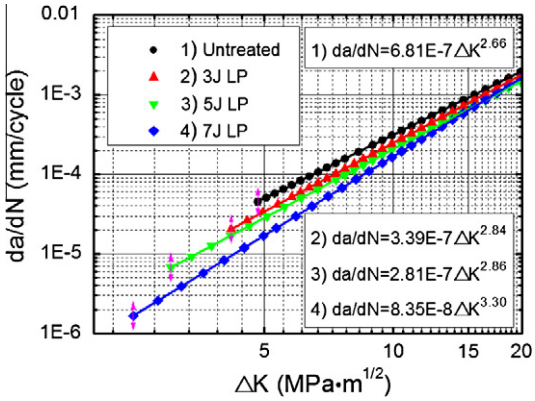

Fig. 15. Numerical curve of the SIF range ΔK versus FCG rate da/dN subjected to different laser energy.

6. Conclusions

LP is an effective surface treatment technique for retarding the growth of fatigue crack and improving the fatigue lives of 6061-T6 CT samples. The results can lead to the application of LP for the healing of cracks in the aging aircraft and automotive structures.

(1) Multiple LP impacts have beneficial effects on the RS levels in the superficial layers. The RS at the crack tip changes from tensile to compressive state after LP, and the values as well as influence depth of compressive RS increase with the increase of laser energy.
(2) In order to verify the reduction of FCG rate by microcosmic performance, FCG path and fatigue striations on fracture surface are observed. It indicates that the fatigue striation spacing of laser peened samples is narrower than that of the untreated samples, and fatigue striation spacing decreases with the increase of laser energy, indicating the decrease of FCG rate.
(3) The laser peened samples result in a reduction of FCG rate when compared with the untreated samples. Meanwhile, the reduction of FCG rate is more evident in the laser peened samples with higher laser energy, which could be attributed to the introduction of higher compressive RS. In addition, the FCG rate reduces obviously by compressive RS in initial stage of FCG. However, the strengthening effects are weak in final period of FCG since the RS releases as the crack grows.
(4) The numerical model of FCG rate and FCG lives under compressive RS is established, reasonable agreements have been obtained between the numerical and experiment results, while further work should be carried out and more accurate prediction model should be studied.

Acknowledgements

The authors are grateful for the support provided by the National Natural Science Foundation of China (No. 51175236), the Research Fund for the Doctoral Program of Higher Education of China (No. 20123227110022), the Key Laboratory Foun-

dation of Photon Manufacturing Science and Technology of Jiangsu Province (No. GZ201107), the Natural Science Foundation of Jiangsu Province (No. BK2010351) and A Project Funded by the PAPD of Jiangsu Higher Education Institutions.

References

[1] Lados DA, Apelian D. Relationships between microstructure and fatigue crack propagation paths in Al–Si–Mg cast alloys. Engng Fract Mech 2008;75:821–32.
[2] Joel JS. Fatigue crack propagation in 7050-T7451 plate alloy. Engng Fract Mech 2009;76:1037–48.
[3] Farrahi GH, Majzoobi GH, Hosseinzadeh F, Harati SM. Experimental evaluation of the effect of residual stress field on crack growth behaviour in C(T) specimen. Engng Fract Mech 2006;73:1772–82.
[4] Zhao JF, Zhou JZ, Huang S, Jiang SQ, Fan YJ. Numerical simulation on fatigue crack growth of metal sheet induced by laser shot peening. Int J Mod Phys B 2009;23:1646–51.
[5] Montross CS, Wei T, Ye L, Clark G, Mai YW. Laser shock processing and its effects on microstructure and properties of metal alloys: a review. Int J Fatigue 2002;24:1021–36.
[6] Lu JZ, Luo KY, Zhang YK, Cui CY, Sun GF, Zhou JZ, et al. Grain refinement of LY2 aluminum alloy induced by ultra-high plastic strain during multiple laser shock processing impacts. Acta Mater 2010;58:3984–94.
[7] Zhang XC, Zhang YK, Lu JZ, Xuan FZ, Wang ZD, Tu ST. Improvement of fatigue life of Ti–6Al–4V alloy by laser shock peening. Mater Sci Engng A 2010;527:3411–5.
[8] Zhou JZ, Huang S, Sheng J, Lu JZ, Wang CD, Chen KM, et al. Effect of repeated impacts on mechanical properties and fatigue fracture morphologies of 6061-T6 aluminum subject to laser peening. Mater Sci Engng A 2012;539:360–8.
[9] Tan Y, Wu G, Yang JM, Pan T. Laser shock peening on fatigue crack growth behaviour of aluminium alloy. Fatigue Fract Engng Mater Struct 2004;27:649–56.
[10] Zou SK, Wang J, Wang HM, Han HJ, Wang CS. Study on laser shock processing to decrease the fatigue crack growth rates of aluminium alloy. Aeronaut Man Technol 2002;9:30–2 [in Chinese].
[11] Rubio-Gonzalez C, Felix-Martinez C, Gomez-Rosas G, Ocana JL, Morales M, Porro JA. Effect of laser shock processing on fatigue crack growth of duplex stainless steel. Mater Sci Engng A 2011;528:914–9.
[12] Rubio-Gonzalez C, Ocana JL, Gomez-Rosas G, Molpeceres C, Paredes M, Banderas A, et al. Effect of laser shock processing on fatigue crack growth and fracture toughness of 6061-T6 aluminum alloy. Mater Sci Engng A 2004;386:291–5.
[13] Liu Q, Yang CH, Ding K, Barter SA, Ye L. The effect of laser power density on the fatigue life of laser-shock-peened 7050 aluminium alloy. Fatigue Fract Engng Mater Struct 2007;30:1110–24.
[14] Luong Harold, Hill Michael R. The effects of laser peening on high-cycle fatigue in 7085-T7651 aluminum alloy. Mater Sci Engng A 2008;477:208–16.
[15] Chahardehi A, Brennan FP, Steuwer A. The effect of residual stresses arising from laser shot peening on fatigue crack growth. Engng Fract Mech 2010;77:2033–9.
[16] Zhang YK, Ren XD, Zhou JZ, Lu JZ, Zhou LC. Investigation of the stress intensity factor changing on the hole crack subject to laser shock processing. Mate Des 2009;30:2769–71.
[17] Peyre P, Carboni C, Forget P, Beranger G, Lemaitre C, Stuart D. Influence of thermal and mechanical surface modifications induced by laser shock processing on the initiation of corrosion pits in 316L stainless steel. J Mater Sci 2007;42:6866–7.
[18] Ye C, Liao YL, Cheng GJ. Warm laser shock peening driven nanostructures and their effects on fatigue performance in aluminum alloy 6160. Adv Engng Mater 2010;12(4):291–7.
[19] Ioannis B, David D, Trevor CL. The role of microtexture on the faceted fracture morphology in Ti–6Al–4V subjected to high-cycle fatigue. Acta Mater 2010;58:3908–18.
[20] Ruschau JJ, John R, Thompson SR, Nicholas T. Fatigue crack nucleation and growth rate behavior of laser shock peened titanium. Int J Fatigue 1999;21:S199–209.
[21] Ren XD, Zhan YK, Zhou JZ, Lu JZ, Zhou LC. Influence of compressive stress on stress intensity factor of hole-edge crack by high strain rate laser shock processing. Mater Des 2009;30:3512–7.
[22] Hatamleh O. Comprehensive investigation on the effects of laser and shot peening on fatigue crack growth in friction stir welded AA 2195 joints. Int J Fatigue 2009;31:974–88.
[23] Bussu G, Irving PE. The role of residual stress and heat affected zone properties on fatigue crack propagation in friction stir welded 2024-T351 aluminum joints. Int J Fatigue 2003;25:77–88.
[24] Maawad E, Sano Y, Wagner L, Brokmeier HG, Genzel C. Investigation of laser shock peening effects on residual stress state and fatigue performance of titanium alloys. Mater Sci Engng A 2012;36:82–91.
[25] Prime MB, Gnaupel-Herold T, Baumann JA, Lederich RJ, Bowden DM, Sebring RJ. Residual stress measurements in a thick, dissimilar aluminum alloy friction stir weld. Acta Mater 2006;54:4013–21.
[26] Fabbro R, Fournier J, Ballard P, Devaux D, Virmont J. Physical study of laser-produced plasma in confined geometry. J Appl Phys 1990;68:775–84.
[27] Johnson JN, Rhode RW. Dynamic deformation twinning in shock loaded iron. J Appl Phys 1971;42:4171–82.
[28] Rankin JE, Hill MR, Hackel LA. The effects of process variations on residual stress in laser peened 7049 T73 aluminum alloy. Mater Sci Engng A 2003;349:279–91.
[29] Peyre P, Fabbro R. Laser shock processing: a review of the physics and applications. Opt Quant Electron 1995;27(12):1213–29.
[30] Ballard P. Residual stress induced by rapid impact-application of laser shocking. Doctorial thesis. France: Ecole Polytechnique; 1991.
[31] Paris PC, Erdogan F. A critical analysis of crack propagation laws. J Basic Engng 1963;85(4):528–34.
[32] Ren XD, Zhang YK, HunagFu YZ, Ruan L, Jiang DW, Zhang T, et al. Effect of laser shock processing on the fatigue crack initiation and propagation of 7050-T7451 aluminum alloy. Mater Sci Engng A 2011;528:2899–903.
[33] Gao YK. Improvement of fatigue property in 7050-T7451 aluminum alloy by laser peening and shot peening. Mater Sci Engng A 2011;528:3823–8.
[34] Zhuang WZ, Halford GR. Investigation of residual stress relaxation under cyclic load. Int J Fatigue 2001;23:S31–7.
[35] Nikitin I, Altenberger I. Comparison of the fatigue behavior and residual stress stability of laser-shock peened and deep rolled austenitic stainless steel AISI 304 in the temperature range 25–600 °C. Mater Sci Engng A 2007;465:176–82.
[36] Juijerm P, Altenberger I. Effect of temperature on cyclic deformation behavior and residual stress relaxation of deep rolled under-aged aluminium alloy AA6110. Mater Sci Engng A 2007;452–3:475–82.